Scanning Microscopy

Volume 2 | Number 2 Article 16

3-15-1988

Scanning Electron Acoustic Microscopy Studies of III-V Compounds: Epitaxial Layers and Devices

J. F. Bresse
Centre National d'Etudes des Telecommunications Laboratoire de Bagneux

Scanning Microscopy, Vol. 2, No. 2, 1988 (Pages 813-819)
Scanning Microscopy International, Chicago (AMF O'Hare), IL 60666 USA

0891-7035/88$3.00+.00

SCANNING ELECTRON ACOUSTIC MICROSCOPY STUDIES OF III-V COMPOUNDS: EPITAXIAL LAYERS AND DEVICES

J. F. Bresse

Centre National d'Etudes des Telecommunications
Laboratoire de Bagneux, Division PMM, Department MPD
196 Avenue Henri Ravera, 92220 Bagneux, France

(Received for publication March 06, 1987, and in revised form Mar. 15, 1988)

Abstract

Scanning electron acoustic microscopy (SEAM) can be used as a tool to visualize integrated circuit failures caused by lithographic processes, metallic overlayer adherence problems, major subsurface defects, and presence of alloyed compounds formed between ohmic contacts and epitaxial layers. Major defects and doping striations are also visualized by SEAM. For highly doped epitaxial layers a dependence has been found between the doping level and the electron acoustic signal.

Key Words : Scanning electron acoustic microscopy, semiconductors, gallium arsenide, indium phosphide, III-V compounds, ohmic contacts.

Address for correspondence :
J. F. Bresse,
Centre National d'Etudes des Telecommunication,
Laboratoire de Bagneux,
Division PMM - Department MPD,
196 Avenue Henri Ravera,
92220 Bagneux, France
Phone : 33-1 45.29.52.43.

Introduction

Scanning electron acoustic microscopy (SEAM) has now become a technique that is easy to implement in a SEM. Commercial systems can be fitted on most microscopes [(e.g, Therma Wave, Inc., Fremont, CA, USA (although Therma Wave, Inc. no longer manufactures an electron acoustic accessory), and Cambridge Technology Ltd., Cambridge, England]. A PZT [composition Pb (Zr, Ti)O_3] transducer can be used at operating frequency up to several MHz. SEAM technique is based on local probing of the thermal properties of metals [4, 5, 8] and of piezoelectric coupling or generated excess carrier recombination in piezoelectric and semiconductor materials [12].

Areas of application of SEAM in semiconductors include: doped area imaging in silicon [14], major surface defects [1], subsurface defects [16], dislocation lattices [17], crystalline lattice perturbation after ion or proton bombardment [10, 16], and grain boundary imaging in solar cells [3, 13]. SiO_2/Si layers with different thicknesses have been visualized because of the large difference between SiO_2 and Si thermal conductivities [8]. Ohmic contacts and Schottky barriers on GaAs substrates have also been studied [11].

SEAM is a powerful tool for studying semiconductor device failures. Several unique possibilities have been shown, for example, imaging of features under an oxide layer [14]. The use of a shift of the detection phase allows one to visualize in depth [2, 15]. This information can be obtained by no other method except in some cases by scanning acoustic microscopy [9].

We present some examples of visualization in epitaxial layers and devices with ohmic contacts. We also show that introduction of dopant impurities gives rise to important signal variations which can be quantified.

Physical phenomena

SEAM is based on local excitation of the sample surface by a periodical pulse causing local periodic heating. The corresponding heat diffusion can be modeled by the development of a thermal wave [6] which does not propagate beyond one wavelength due to excessive dampening. The solution of the heat diffusion equation shows that this thermal wave is attenuated by a factor e after propagation of one thermal diffusion length, μ ($\mu = \lambda/2\pi$), where λ is the thermal wave-length. Thermal

diffusion length can be expressed as:

$$\mu = (K'/\pi f)^{\frac{1}{2}} \quad (1)$$

where:
$K' = K/\rho C$,
K': thermal diffusivity (cm^2/s)
K : thermal conductivity (cal/cm/sec/°C)
ρ : density (gm/cm^3)
C : specific heat (cal/g/°C)
f : frequency

In spite of their high attenuation, the thermal waves have the same characteristics as conventional waves. In particular, they can be scattered or deflected. That is why they can be used to image features with different thermal properties. In piezoelectric and semiconductor materials, it is difficult to establish that the heating is the main phenomenon. Nevertheless the mathematical treatment of the problem is similar and the local character of the emission is still valuable [12]. The spatial resolution, d, attainable by this technique depends on the electron beam spot size, ϕ_b, the total electron penetration, R, and the thermal diffusion length, (because the phenomena are independent):

$$d = (\phi_b{}^2 + R^2 + \mu^2)^{1/2} \quad (2)$$

The electron penetration can be calculated using Kanaya's formula [10]:

$$R(\mu m) = 2.76\ 10^{-2}\ \rho^{-1}\ A\ Z^{-8/9}\ Eo(keV)^{5/3} \quad (3)$$

Thermal diffusion length at a frequency is calculated using Handbook's data on thermal conductivities [7].

Table 1 shows the values of spatial resolution. For a stress-free surface heated by a temperature pulse with frequency f and a power density P_o ($watt/cm^2$), the elastic energy conversion is given by [18] :

$$\eta = I_{elastic}/I_{absorbed} \quad (4)$$

so
$$\eta = \frac{8\Pi}{J^2} \times \frac{B^2 a^2 K'^3}{\rho v^5 K^2} \times P_o \times f \quad (5)$$

where:
B : bulk modulus ($dynes/cm^2$)
a : linear dilatation coefficient
J : mechanical equivalent of heat
v : sound velocity (cm/s)

Table 1 also shows the calculated energy conversion efficiencies for metals and semiconductors.

As a general remark, metals, which have better electrical and thermal conductivities give higher efficiencies than semiconductors and insulators. Nevertheless efficiencies are very low in semiconductors. The signal detection requires sophisticated electronics and sufficient beam current in order to increase the beam power density. As stated by White's formula [18] the efficiency is proportional to the thermal conductivity. Minor changes such as doping variations in semiconductors do not induce change in structural properties, i.e., no change in dilatation coefficient, bulk modulus, and sound velocity, but cause an increase in the thermal conductivity, which is followed by an increase in the electron acoustic efficiency.

Table 1: Attainable resolution [at 1 MHz frequency (beam conditions: sport size (1 μm), energy 20 and 40 keV)] and efficiency [beam conditions: energy 20 keV, current 10^{-7} A, spot size 1 μm (P_o = 2.54 x 10^5 W/cm_2)].

Material	μ(μm) at 1MHz	d (μm) 20 keV	d (μm) 40 keV	η
Al	1.2	4.4	13.3	$6.2\ 10^{-9}$
Si	5.4	7.2	15.9	
SiO_2	0.44	4.9	15.2	
Ti	1.6	3.4	9.0	$2.1\ 10^{-11}$
Ni	3.95	4.3	6.0	$1.1\ 10^{-8}$
Zn	4.8	5.2	7.6	$6.5\ 10^{-9}$
Cu	6.0	6.3	7.6	$2.0\ 10^{-9}$
GaAs	2.8	3.8	8.5	$3.2\ 10^{-11}$
InP	3.8	4.8	9.8	$3.8\ 10^{-11}$
Ge	3.4	4.3	8.8	
Ag	7.5	7.6	7.7	$1.4\ 10^{-8}$
Sn	3.5	4.5	9.0	$2.6\ 10^{-9}$
Pt	2.8	3.0	3.6	$5.2\ 10^{-10}$
Au	6.4	6.5	7.0	$2.4\ 10^{-9}$

Experimental set-up

Experiments were performed using a Cambridge Technology Limited system. A connector has been adapted to the sample holder in order to allow the use of an airlock system. The system can be operated between 10 kHZ and 2 MHz. The electrostatic beam blanking (JEOL BBD-40) fitted to our microscope (JEOL 840 LGS) can work with 1 nsec risetime and deliver electron beam peak current as high as 10^{-5}A at 40 keV. The experiments have been performed at the resonance frequency of the PZT transducer. An autoramp movement is used for the selection of the operating frequency which has to be adjusted with good accuracy to follow the resonance of the sample transducer assembly. An accuracy of 10 Hz in the range 100 kHz-500 kHZ is usually achieved. A low time constant (of 10^{-4} sec) is used on the lock-in amplifier to obtain direct imaging on the CRT without the use of a frame store. The samples are directly glued on the transducer using aquadag. Samples are usually not greater than 5 x 5 x 1 mm^3.

Epitaxial layers

Epitaxial layers of the same composition as the substrate can be grown by liquid phase epitaxy, organometallic epitaxy, or molecular beam epitaxy (MBE). Dopant can be incorporated in the layers

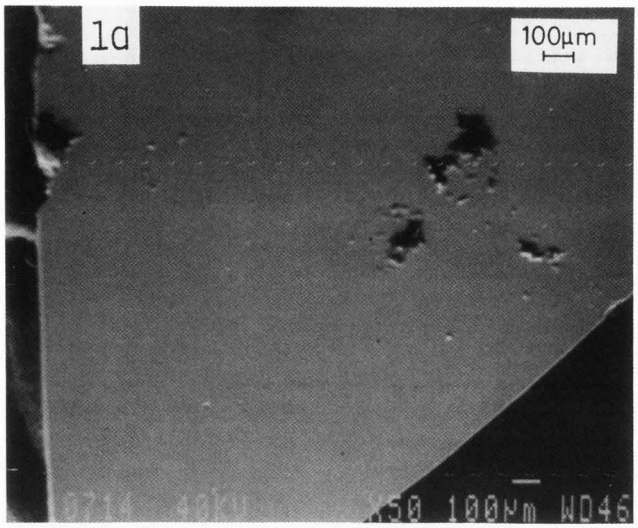

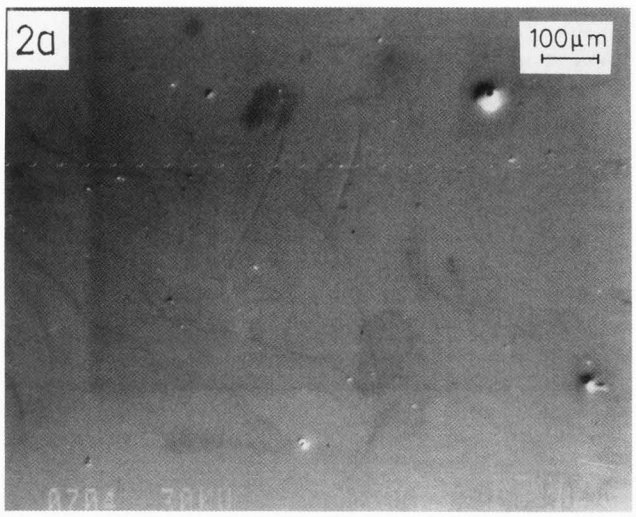

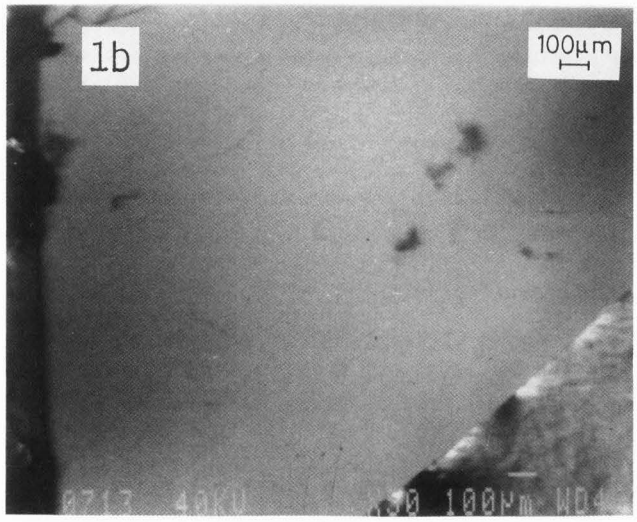

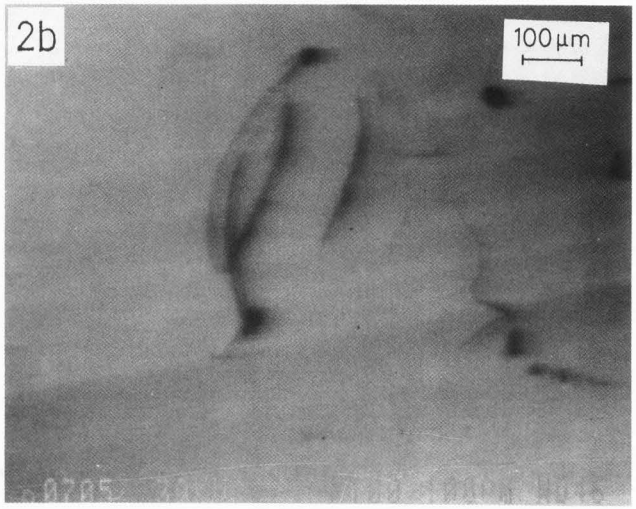

Figure 1. a) Secondary electron image, and b) electron acoustic image (frequency 242 KHz) of sample A ($N_A = 10^{19}$ at.cm^{-3}).
Figure 2. a) Secondary electron image, and b) electron acoustic image (frequency 242 KHz) of sample B ($N_A = 10^{20}$ at.cm^{-3}).

during the growth to prepare buffer layers which are used in the processing of devices such as field effect transistors, laser diodes, heterojunction bipolar transistors etc..

GaAs: Be epitaxial layers have been grown by MBE with doping levels up to 10^{20} at.cm^{-3} (growth conditions: substrate temperature 600°C, V/III ratio during growth 15). The thickness of layers is 5 µm. When these layers are excited by the electron beam at 20 keV beam energy, 1 µA beam current, the total spread and the thermal diffusion length is around 6 µm at 250 kHz operating frequency. So the generated thermal waves are almost localized in the epitaxial layers. Figs. 1 and 2 show, for two samples A and B, the secondary electron image (SEI) giving the surface topography; and the electron acoustic image (EAI) at 242 kHz.

For the sample A($N_A = 10^{19}$ at.cm^{-3}) a few linear defects are observed in the epitaxial layer (scanned area 2 x 2 mm^2). For sample B($N_A = 10^{20}$ at.cm^{-3}) a great number of extended defects are observed (scanned area : 1 x 1mm^2). Most of the defects propagate along the total depth of the epilayer and give a strong contrast. In addition, striations are observed in sample B which are all in the same crystallographic direction. These doping striations may be related to the lattice mismatch between the epilayer ($Ga_{0.99}Be_{0.01}As$ alloy) and the substrate.

Devices

Imaging of doped areas lithographic problems

Usually the delineation of zones where diffusion, ion implantation occurs is preliminarily defined by a masking process and the transfer is made using a photoresist. Doped layers can be visualized by the electron acoustic image. Defects

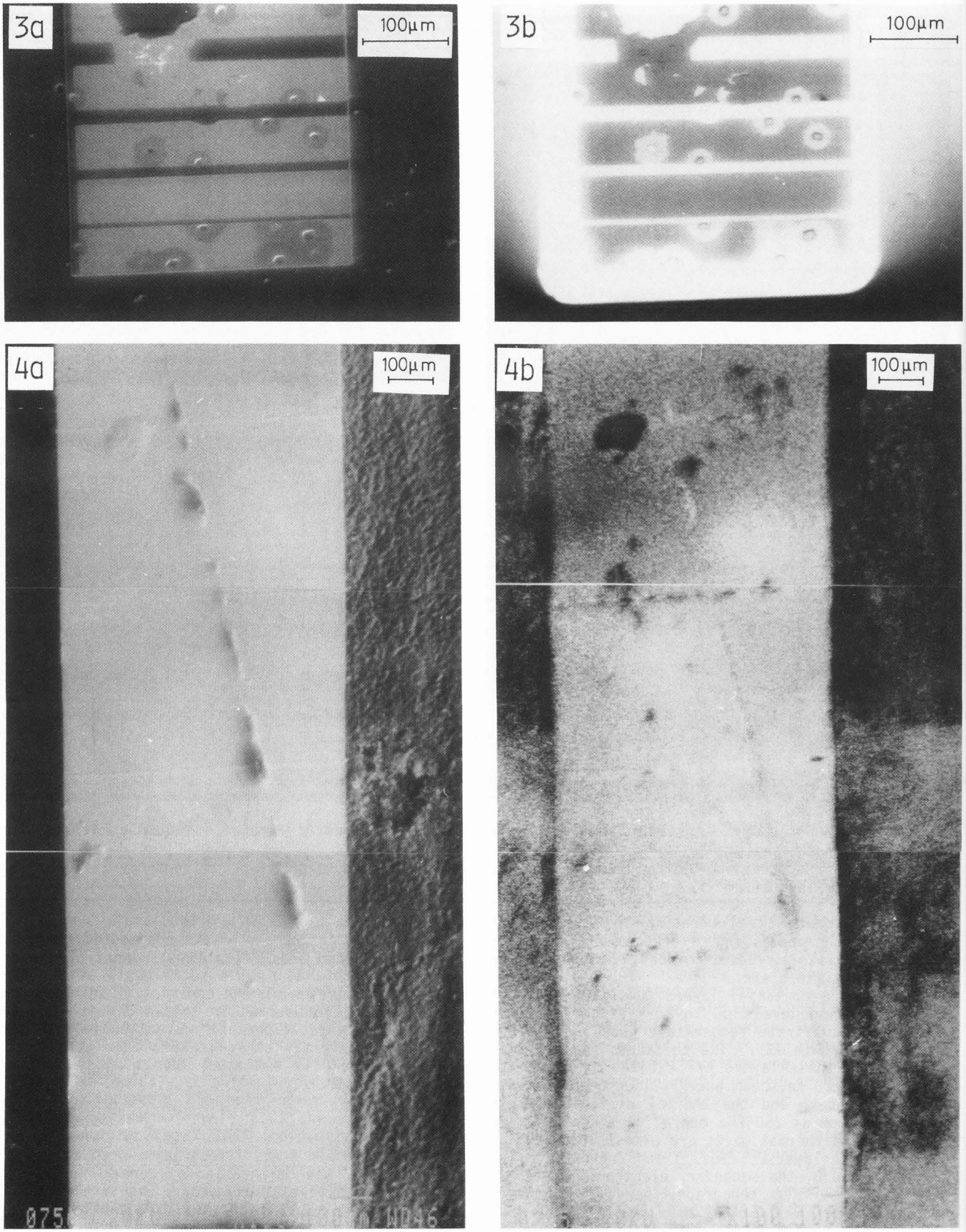

Fig. 4 a) secondary electron image, and b) electron acoustic image (frequency 214 KHz) of a bar of lasers.

Fig. 3 (facing page, top) a) secondary electron image, and b) electron acoustic image (frequency 243 KHz) of mesa structure with contacts Mo-Ge/GaAs.

in the lithographic process can thus be revealed by an irregular extension of the doped area. Figs. 3 a) and b) show an example for a mesa structure with ohmic contacts on the top. These ohmic contacts (structure Mo-Ge/GaAs) have shown very low resistivities and a good adherence without the formation of compounds at the interface contact/substrate.

The mesa shape has been delineated by a lithographic process. As shown on the image the extent of doped area is given by the lithographic process. We also can notice that the dopant is uniformly distributed and this uniformity can be probed even below the ohmic contact.

Ohmic contacts

Ohmic contact formation is one of the most significant problems in III-V compound devices. The metallurgical process involved in contact formation can cause adherence problems, and interface compound formation between the metal and the semiconductor giving rise to island conduction.

Adherence problems Lasers usually have a multilayer metallic contact structure to ensure good heat dissipation when the metallic face is in contact with the chip holder. For the bar of laser diodes, presented in Figure 4, laser diodes are separated by 0.4 mm. The laser has a mesa shape and an ohmic contact (alloy Au-Zn, 0.2 μm thick) has been formed on the top of the mesa and is 8 μm wide. An overlayer (Au 200 nm, Ti 40 nm) has been deposited on the entire surface to ensure a good heat conduction.

One bubble is observed on the SEI (upper-left corner) which gives a strong contrast in EAI due to the absence of contact between the metal and the semiconductor. All the dark zones observed on the EAI reveal adherence problems between the overlayer and the semiconductor.

Interface compound formation Fig. 5 shows an example of interface compound imaging. The structure of ohmic contact is Au-Zn alloy (0.2 μm)/GaAs. At 20 keV, the electron beam energy is mainly dissipated in the ohmic contact. An interface compound situated below the metallic layer begins to be imaged due to its different thermal conductivity properties. At 40 keV the electron beam penetrates more deeply in the metallic layer and the interface compound is visualized with a resolution which is mainly governed by the thermal diffusion length in the GaAs substrate (see top left of Fig. 5C).

Relationship between electron-acoustic signal and doping level

As the doping level is increased, the resulting changes in electrical and thermal conductivity may affect the electron acoustic efficiency. In order to find a relationship between the electron acoustic signal and the doping level we have done the following experiments. For the measurements some precautions have to be taken. The sample is cut in a small piece (less the 5 x 5 mm x 0.3 mm^3) and carefully glued on the PZT transducer. The electron acoustic signal is measured at the output of the preamplifier. Constant beam energy and beam

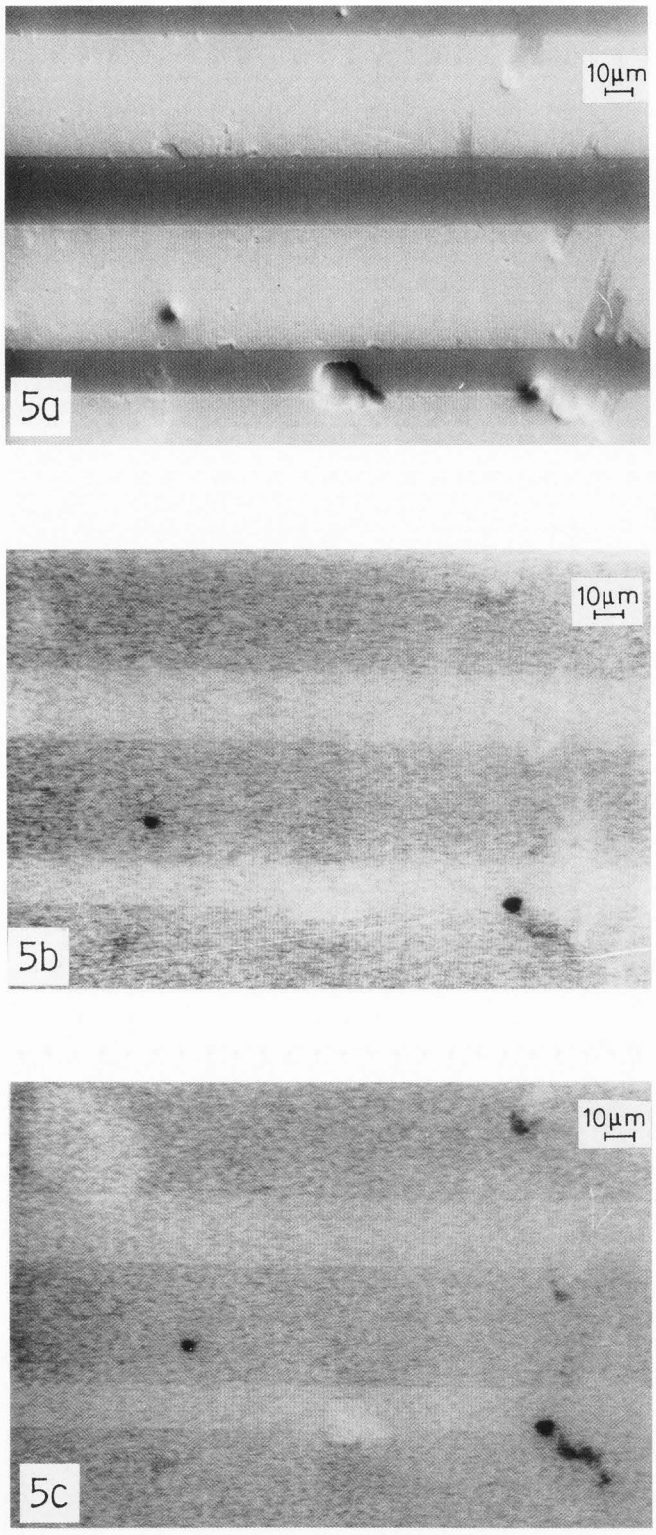

Fig. 5 a) secondary electron image, b) and c) electron acoustic images (frequency 221 KHz) at beam energies of 20 keV (Fig. 5b) and 40 keV (Fig. 5C) of ohmic contacts Au-Zn/GaAs..

current are used during the experiments. The operation frequency is very precisely adjusted to obtain the maximum signal response around the resonance frequency of the transducer (250 kHz in our case). The layers on which the measurements have been made are several μm thick; thus all the thermal waves are mainly confined in the layers. Electron acoustic response has been measured for several types of doped layers: 5 μm thick GaAs : Be layers with doping levels varying form 6.5×10^{17} to 10^{20} at.cm^{-3}; 1 μm thick $Ga_{0.28}Al_{0.19}In_{0.53}As$: Si layers with doping levels from 8.0×10^{16} to 6.5×10^{18} at.cm^{-3}; 1 μm thick GaAs : Si layers with doping levels varying from 1.0×10^{17} to 6.3×10^{18} at.cm^{-3}. Fig. 6 shows the evolution of the electron acoustic signal as a function of the doping level at following beam conditions: current (in all cases) = 2 μA; and energy = 20 keV for GaAs : Si and $Ga_{0.28}Al_{0.19}In_{0.53}As$: Si layers, and energy = 40 keV for GaAs : Be layers.

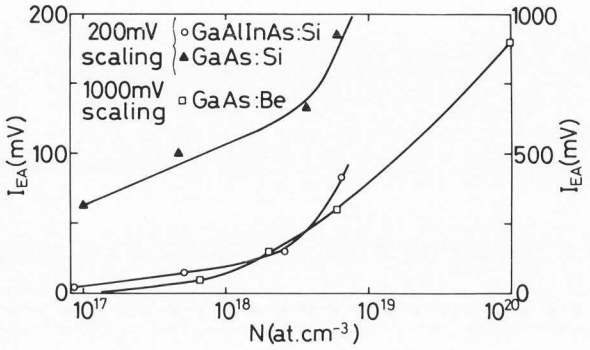

Fig. 6 Electron acoustic signal as function of doping level.

The beam energy has been chosen to allow good penetration in the layers. From the curves in Fig. 6, we notice that the evolution of the electron acoustic signal, as function of the doping level, is the same for the three types of layers. The doping level measured by the Hall effect represents the electrically active concentration of dopant. In the case of $Ga_{0.28}Al_{0.19}In_{0.53}As$: Si, a cathodoluminescence study of these epitaxial layers (Papadopoulo AC, Bresse JF, Preseuth JP, J. Appl. Phys. in press) has shown that the dopant incorporation is donor-acceptor type. But for a doping level greater than 10^{18} at.cm^{-3} a parallel increase of deep level concentration is observed which is related to the presence of silicon complexes. Above this doping level, a decrease of intensity of the donor-acceptor transition is observed. From this complementary study we can conclude that the electron acoustic signal follows, for a low doping level, the evolution of the donor-acceptors which give the conductivity, and for a high doping level, an evolution which sums the conductivity given by the donor-acceptor and deep level concentrations including non-radiative phenomena. The evolution of the electron acoustic signal appears to be influenced by the material, the nature of dopant, and the growth conditions. These three factors should define a calibration curve for a sample with unknown doping level grown in the same experimental conditions. In the present state the accuracy of the measurements only permits an estimation of the doping level.

Conclusions

We have shown the application of SEAM for imaging major subsurface defects, doped areas with or without metallic layers, doping striations in epitaxial layers, and formation of compounds at ohmic contact metal interface. These applications correspond to a wide open field for device failure diagnostic. Furthermore we also point out a quantitative relationship between the SEAM signal and the free carrier concentration.

Acknowledgements

The authors wish to thank J. L. Lievin, J. P. Praseuth for growing the MBE epitaxial layers, C. Dubon-Chevallier for GaAs devices with ohmic contact, J. C. Bouley for laser diodes.

References

1. Balk LJ, Kultscher N (1984). Nonlinear Scanning electron acoustic microscopy. J. Physique 45 (2), C2-869-872.

2. Balk LJ, Kultscher N (1984). Scanning electron acoustic microscopy with subnanosecond time resolution. J. Physique 45 (2), C2-873-876.

3. Balk LJ, Richard G, Kultscher N (1985). Semiconductor characterization by simultaneous evaluation of electron beam induced current and scanning electron microscope. Inst. Phys. Conf. Ser. No.76, Institute of Physics, Bristol U.K., 342-349.

4. Brandis E, Rosencwaig A (1980). Thermal wave microscopy with electron beams. Appl. Phys. Lett. 37, 98-100.

5. Cargill III GS (1980). Ultrasonic imaging in scanning electron microscopy. Nature 286, 691-693.

6. Carlaw HS, Jaeger JC (1973). In : Conduction of Heat in Solids, 2nd edition, Oxford University Press, U.K., 64-70.

7. CRC Handbook of Chemistry and Physics (1983). 63rd Edition. Weast RC, Astle MJ (Eds.), CRC Press Inc, Boca Raton, Florida.

8. Davies DG (1983). Scanning electron acoustic microscopy. Scanning Electron Microsc. 1983;III : 1163-1176.

9. Jipson V, Quate CF (1978). Acoustic microscopy at optical wavelengths. Appl. Phys. Lett. 32, 789-791.

10. Kanaya K, Okoyama S (1972). Penetration and energy loss theory of electrons in solid targets. J. Phys. D 3, 43-58.

11. Kirkendall TD, Remmel TP (1984). Thermal wave imaging of GaAs material and devices. J. Physique 45 (2), C2-877-880.

12. Kultscher N, Balk LJ (1986). Signal generation mechanisms in scanning electron acoustic microscopy. Scanning Electron Microsc. 1986;I : 33-43.

13. Marek J, Strausser YE (1984). Correlation of thermal wave imaging to other analysis methods. Appl. Phys. Lett. 44, 1152-1154.

14. Rosencwaig A, White RM (1981). Imaging of dopant regions in silicon with thermal-wave elec-

tron microscopy. Appl. Phys. Lett. 38, 165-167.

15. Rosencwaig A (1982). Thermal wave imaging Science, 218, 223-228.

16. Rosencwaig A (1984). Thermal wave imaging in a scanning electron microscope. Scanning Electron Microsc. 1984;IV : 1611-1628.

17. Takenoshita H, Managaki M, Mizuno K (1985). Observation of dislocation lines in a transistor by electron-acoustic microscopy. Proceedings 5th Symposium on Ultrasonic Electronics, Tokyo, Jap. J. Appl. Phys, 24, Suppl 24-1, 93-96.

18. White RM (1963). Generation of elastic waves by transient surface heating. J. Appl. Phys., 34, 3559-3567.

Discussion with Reviewers

T. Kirkendall: Why were two acceleration voltages (i.e., 20 keV and 40 keV) used to generate the response of the electron acoustic signal as a function of doping level in 3 compounds?
Author: The electron beam energy is adjusted in order to give an electron penetration through the epitaxial layer of each compound. So the SEAM signal concerns the total layer thickness by the combined effect of beam penetration and thermal diffusion length.

H. Takenoshita: What was:
a) the time of one frame scan;
b) the number of raster lines;
c) absorbed currents in EAIS; and
d) resolution power in EAIS?
Author: The time for one scan is 100 sec, with 240 msec per line so the number of lines is 420. The electron beam current is between 0.5 to 2 x 10^{-6} A so the absorbed current is just a fraction of these values. The resolution power is determined by the beam spot size, the electron range, and the thermal diffusion length. At an operation frequency of 250 kHz, a beam spot size of 1 μm we expect a resolution about 6 μm at 20 keV in low doped GaAs and around 3 μm for heavily doped GaAs.

H. Takenoshita: Have you performed observations with other SEM modes such as characteristics X-ray images or EBIC images under different bias conditions?
Author: Our apparatus is also designed for cathodoluminescence at low temperature which can give same information on electrical properties, as EBIC, without the need of a metallic contact. We are expecting to do both experiments on the same samples in the future.

H. Takenoshita: To what extent will the thermal properties of the specimen change, when the doping level is increased form 10^{17} to 10^{20} at.cm^{-3}?
Author: The lattice contribution to the thermal conductivity is given by the formula:

$$K_L = (1/3)\ C\ v\ l$$

where: C is the specific heat, v the sound velocity, l the mean free path between collisions. For doping levels varying form 10^{17} to 10^{20} at.cm^{-3}, the mean free path decreases by a factor of 10, giving a decrease in thermal conductivity by a factor of 10. The electronic contribution to the thermal conductivity is estimated, by calculations, to give a very small increase.

S. Utterback: Since the coupling between the thermal source and the acoustic wave calculated by equation (4) shows better coupling for metals than insulators, insulators tend to get much hotter thus expanding more. Experimentally, how did the acoustic signal intensity vary going from conductors to insulators (independent of detectors, non-thermal acoustic generation effects, etc.).
Author: The electron acoustic signal is a function of such parameters as: bulk modulus, linear expansion coefficient, density, sound velocity, thermal conductivity, and specific heat. The combination of all these parameters explains the difference of response between metals and insulators.

S. Utterback: Please provide a more detailed explanation as to the acoustic signal contrast mechanisms in the case of doped regions?
Author: Dopant and point defects, which cause a disruption of the lattice structure of the material, cause a change in local thermal conductivity. This can explain the contrast mechanism which permits us to visualize doped regions.

S. Utterback: How did the observed resolution compare to the calculated resolution?
Author: The calculated resolution, at an operating frequency of 250 kHz, is 5.6 μm for undoped GaAs and less than 2 μm for heavily doped GaAs (about 10^{18} at. cm^{-3}). The observed resolution, for example, in the case of doped layers (doping level 10^{18} at. cm^{-3}, see Fig. 6b) is of the same order of magnitude.